THE JOURNAL OF PHYSICAL CHEMISTRY C
A JOURNAL OF THE AMERICAN CHEMICAL SOCIETY

pubs.acs.org/JPCC

Article

Pump-Selective Spectral Shaping of the Ultrafast Response in Plasmonic Nanostars

Andrea Schirato,[†] Luca Moretti,[†] Elisa Lacroce, Laura Polito, Filippo Rossi, Giuseppe Della Valle, and Margherita Maiuri*

Cite This: *J. Phys. Chem. C* 2024, 128, 2551−2560

Read Online

ACCESS | Metrics & More | Article Recommendations | Supporting Information

ABSTRACT: Plasmonic nanostructures are, to date, well-known to offer unique possibilities for the tailoring of light−matter interactions at the nanoscale. Most recently, a new route to ultrafast all-optical modulation has been disclosed by combining the resonant features of plasmonic nanostructures with the giant third-order optical nonlinearity of noble metals regulated by highly energetic (hot) carriers. In this framework, a variety of nanostructures have been designed, with special attention to shapes featuring tips, where extreme and highly sensitive field enhancements (hot spots) can be attained. Here, we report on a broadband pump−probe spectroscopy analysis of an ensemble of spiky star-shaped nanoparticles, exploring both the perturbative and nonperturbative regimes of photoexcitation. The experiments are corroborated by semiclassical numerical simulations of the ultrafast optical response of the sample. We found that the peculiar hot spots supported by the star tips allow one to easily control the spectral shape of the transient optical signal, upon tuning of the pump wavelength. Our results elucidate the ultrafast response of hot electrons in star-shaped nanostructures and contribute to the understanding of the tip-mediated enhanced nonlinearities. This work paves the way to the development of ultrafast all-optical plasmonic modulators for pump-selective spectral shaping.

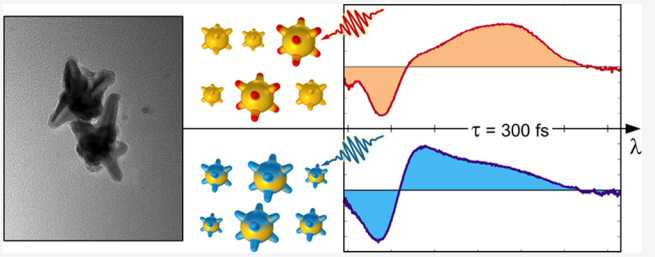

INTRODUCTION

Plasmonic nanostructured materials offer a unique route for interacting with light at the nanoscale.[1−3] These metal structures can indeed couple strongly to the electromagnetic radiation and exhibit a driven oscillation of their free electrons, known as localized surface plasmon resonance (LSPR).[4] The spectral position, width, and intensity of the LSPR are highly sensitive to the nanoparticle (NP) shape, size, material, and surrounding environment, while the number of resonant modes across the spectrum is mostly determined by geometrical aspects (i.e., the shape, in case of isolated NPs, or the spatial arrangement, when NPs are coupled).[5,6] Such an inherent property of plasmonic systems explains the development of nano-objects with growing structural complexity, starting from rods, dimers, and core−shell particles[7−9] to cubes, hexapods, and more exotic shapes,[10−12] which exhibit multimodal, easy-to-tune optical responses, thanks to the increased degrees of freedom. Special interest has been given to geometries featuring spikes, tips, and edges such as, e.g., bipyramids, cones, or star-shaped nanoparticles (s-NPs): in the sharpest regions, light excitation produces electromagnetic hot spots where radiation is highly confined and extreme field enhancements can be attained. Because of these intense near fields induced at their hot spots, spiky nanostructures show enhanced sensitivity to their local environment[13] and, as such, have gained great attention, e.g., in surface-enhanced Raman spectroscopy,[14−17] biochemical sensing and applications,[18−20] and surface chemistry.[21−24]

Studying the optical properties of plasmonic NPs with complex morphologies and localized hot spots can be, however, far from straightforward. While being highly attractive from the application standpoint, the tunability and sensitivity to minor shape modifications of these systems are counterbalanced by a significant complexity of their optical behavior. For disordered ensembles such as colloidal solutions, the observed linear optical response depends on the nontrivial superposition of single-object features, which differ for even slight variations of the same NP shape. Therefore, the spectra get congested and harder to interpret, hindering the rational design of NPs and effective exploitation of their hot spots.

Time-resolved nonlinear optical techniques are an ideal tool to disentangle spectral signatures in complex NP systems.[12,25,26] In particular, ultrafast pump−probe spectroscopy measures the dynamical processes taking place in photoexcited systems,[27] which is of particular relevance when dealing with

Received: November 1, 2023
Revised: December 21, 2023
Accepted: January 15, 2024
Published: February 2, 2024

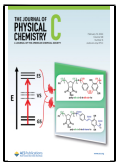

plasmonic nanostructures.[28] The out-of-equilibrium, nonlinear response of metal NPs induced by the intense pump pulse[29] arises from a cascade of intertwined events, governed by the ultrafast relaxation of nonequilibrium "hot" carriers, which follow plasmon dephasing.[30,31] These photoexcited electronic states reach, in the ultrafast regime, energies much higher than those at thermal equilibrium, thus promoting multiple processes otherwise unattainable.[32] As such, characterizing the ultrafast optical behavior of complex-shaped plasmonic NPs, ideally combining experiments with a theoretical description of the phenomena at play, provides a complete, unambiguous picture of the system photophysics.

In this context, s-NPs represent an exemplary nanostructure with a rich optical response that, in principle, can outperform standard geometries. The branched shape gives rise to a multimodal optical response with a high tunability dictated by the star-like geometry, that theory can well explain.[33] However, the predicted features related to the NP tips are most often broadened by the sample synthesis, up to cases where almost only one resonant mode can be observed.[34−36] This tends to limit the experimental investigation and exploitation of the nanostar tips. For instance, theoretical results have shown that s-NPs support photoinduced nonequilibrium carriers at their hot spots, with substantial advantages for photocatalysis compared to spheres and rods.[37,38] Hot electrons photogenerated at the s-NP spikes are also expected to induce strong nonlinearities,[29,39] contributing to the ultrafast optical response. However, while ultrafast coherent lattice oscillations (on time scales from tens to hundreds of ps) of s-NPs have been analyzed,[36] their early time behavior has not been examined yet.

In this work, we investigate the ultrafast optical properties of colloidal plasmonic s-NPs by combining femtosecond pump−probe spectroscopy and semiclassical dynamical modeling. Pump−probe experiments have been performed under two conditions, namely, both off- and on-resonance with the structure tips. In the former case, the response is dominated by the s-NPs whole ensemble, providing insight into the metal intrinsic properties. By analyzing the transient optical signals over a broad range of wavelengths as a function of the fluence, we observe a saturation effect, manifesting as a major distortion in the differential transmittance spectra for increasing pump fluence. The theoretical model explains this phenomenon as the fingerprint of nonequilibrium electron-induced nonlinearities in Au. On the other hand, when the pump pulse is tuned to the tip-mediated resonance, a completely different spectral shape of the transient signals is obtained. The effect is rationalized as a selection process of specific s-NP subsets within the whole ensemble, is ascribed to the nanostructure resonant tips, and indicates the possibility to directly shaping the spectra of the optical signal by tuning the pump wavelength. In its whole, our study aims at elucidating the ultrafast dynamics of photoexcited plasmonic star-shaped NPs, in view of future exploitation of short-lived hot electrons localized at the hot spots and the development of ultrafast nanodevices for pump-selective spectral shaping.

MATERIALS AND METHODS

Sample Preparation. Au s-NPs were synthesized by means of a one-step protocol[40,41] based on the reduction, at room temperature and in aqueous environment, of tetrachloroauric acid ($HAuCl_4$) to Au^0 by using ascorbic acid (AA) as a reductive and preliminary stabilizing agent and subsequent addition of silver nitrate ($AgNO_3$). The s-NP shaping is ruled by the pH, which was set to an optimized value of 3.93, with small deviations from this value leading to either uncontrolled hyperbranched systems or to inhomogeneous morphologies. Our original experimental setup consisted of a benchtop reactor made up of a dual syringe pump (Legato 200, KD Scientific) working at a 5 mL/min flow rate, connected through a PEEK T-mixer to a PTFE tube reaction coil (ID 1 mm, length 160 mm). In a typical procedure, one syringe is loaded with 20 mL of a solution of L-ascorbic acid 0.8 mM and the other one is loaded with 20 mL of a solution containing $HAuCl_4$ 0.2 mM and $AgNO_3$ 0.02 mM. The obtained NPs were directly dropped in a solution containing 3 mg of SH-PEG_{5000}-OCH_3 or 3 mL of sodium citrate solution (1 or 2% v/v) in order to stabilize the colloidal solution. The resulting metal concentration was 0.07 mg/mL.

Pump−probe Spectroscopy. Ultrafast pump−probe spectroscopy experiments were performed using an amplified Ti:sapphire laser (Coherent Libra), generating ∼100 fs pulses with a repetition rate of 1 kHz, centered around 800 nm. The pump pulses at a wavelength of 400 nm were generated by means of frequency doubling in a β-barium borate crystal illuminated by the laser fundamental output. The fluence was varied by almost 1 order of magnitude in order to investigate different perturbation regimes. The pump pulses at 660 nm were generated by means of optical parametric amplification (OPA) in a β-barium borate crystal, amplifying the corresponding white-light supercontinuum portion by means of pumping the crystal with the frequency doubled fundamental beam. The fluence of the OPA pulses was set in order to have a transient signal amplitude comparable with the 400 nm excitation case. White-light supercontinuum generation in a thin sapphire plate was instead exploited to obtain broadband probe pulses, spanning the visible (440−760 nm) spectral region. All measurements were performed with relative perpendicular polarization between pump and probe beams (to minimize pump scattering effects), at room temperature in a 1 mm optical path quartz cuvette.

Numerical Modeling. To simulate the sample linear and nonlinear response, a multistep modeling approach was pursued, combining finite element method (FEM)-based numerical computation with a semiclassical description of the nonlinear photoexcitation of plasmonic structures. For the static optical behavior of the system, a FEM electromagnetic model was developed (using the commercial software COMSOL Multiphysics 6.0), solving Maxwell's equations in the scattering formalism for a single Au s-NP embedded in a homogeneous environment (water, refractive index 1.33). Excitation with monochromatic linearly polarized planewave was considered to determine the sample transmission (for a particle concentration set at the 95% of its nominal value).[42] The s-NP numerical geometry was built as a spherical core surrounded by eight conical spikes in the directions [±1, ±1, ±1], so to obtain an isotropic structure, with dimensions estimated from the transmission electron microscopy (TEM) images of the sample. In particular, a core radius of ∼20 nm and an overall tip-to-tip distance of ∼60 nm were considered. Metal permittivity was described based on the experimental data,[43] where an analytical Drude-like term with increased damping factor Γ was introduced following the approach reported in ref 37, to reproduce the resonance inhomogeneous broadening in the sample. Agreement with experiments was obtained with an 11-fold increased Γ compared to its bulk

https://doi.org/10.1021/acs.jpcc.3c07267
J. Phys. Chem. C 2024, 128, 2551−2560

value.[37] To determine the dynamical response of the sample upon ultrashort pulse excitation, a description of the photogeneration of energetic (hot) carriers and the subsequent relaxation processes was employed, based on the well-established three-temperature model (3TM).[44] This is a rate-equation model detailing the photoexcitation and relaxation of plasmonic nanostructures upon illumination with ultrashort laser pulses in terms of three energetic degrees of freedom: N, the excess energy stored in an out-of-equilibrium nonthermal fraction of the electronic population; Θ_E, the temperature of thermalized hot carriers; and Θ_L, the Au lattice temperature. In light of the peculiar geometry considered, a spatially inhomogeneous formulation of the model[45] was pursued, to account for potential effects of excitation spatial diffusion and heat transfer on the dynamics. For a space- (across the single NP) and time-dependent power density P_{abs} absorbed by the NP, the three variables are interlinked by the following equations[44,45]

$$\frac{\partial N}{\partial t} = -aN - bN + P_{abs} \tag{1}$$

$$C_E \frac{\partial \Theta_E}{\partial t} = -\nabla\cdot(-\kappa_E \nabla \Theta_E) - G(\Theta_E - \Theta_L) + aN \tag{2}$$

$$C_L \frac{\partial \Theta_L}{\partial t} = \kappa_L \nabla^2 \Theta_L + G(\Theta_E - \Theta_L) + bN - \frac{H(t)}{V} \tag{3}$$

where the coefficients above regulate the energy relaxation processes ensuing the photoexcitation. In particular, a and b represent the coefficients governing nonthermalized electrons relaxation via either electron−electron or electron−phonon scattering, respectively; C_E and C_L denote the thermalized electron and lattice heat capacities; κ_E and κ_L denote their thermal conductivities; and G refers to the electron−phonon coupling term. Finally, $H(t)$ is the coupling term accounting for the heat transfer from the metal lattice (V being the NP volume) to its surrounding environment, where a standard Fourier-like equation (not shown here) regulates the temperature field evolution. Further details on our model implementation can be found elsewhere.[45−47] The integration of the 3TM provided us with the dynamics of the (electronic and phononic) energetic variables of the metallic structure, which we combined with a semiclassical model of the thermo-modulational optical nonlinearities in Au[48] to compute the metal permittivity variations transiently photoinduced by pump absorption. Indeed, each of the three energetic degrees of freedom drives broadband changes in Au permittivity, evolving on ultrafast timescales. Both N and Θ_E, modifying the electronic energy occupancy distribution, affect the metal photoabsorption promoted by interband transitions (at the L-point in the first Brillouin zone, in our model), a process described as a modification of the permittivity imaginary part (its real counterpart being given by Kramers−Kronig relations). On the other hand, an increased lattice temperature causes changes in the Drude-like intraband term of Au permittivity, as a result of varied damping factor and plasma frequency. These permittivity calculations were performed by considering the values of the three N, Θ_E, and Θ_L variables averaged over the volume of the single s-NP defined in the FEM model, representative, to the leading order, of the degree of excitation of the structure at each time step. Indeed, given the relatively small size of the effective NP used to reproduce the sample optical response, the optical perturbation is quasi-homogeneous. To finally determine the transient optical response of the perturbed structure in interaction with a broadband delayed probe pulse, a perturbative approach was applied, computing the differential transmission signal as a linear combination of the complex-valued permittivity modulation.

RESULTS AND DISCUSSION

A solution of uniform Au s-NPs was obtained following the chemical synthesis procedure detailed in the Materials and Methods. TEM images of the sample reported in Figure 1a confirm the typical morphology of the NPs, featuring well-defined spikes in the three dimensions with a mean tip-to-tip distance in the range of ∼50−70 nm and estimated core diameters of ∼20−30 nm. TEM analysis of our sample also suggested that (i) s-NPs are far apart (consistently with the relatively low NP concentration), making it licit to consider the system as dominated by the isolated particles' response, disregarding the aggregation effects; and (ii) although there exists an overall uniformity, the solution contains partially diversified star-like shapes (e.g., varied tip morphology), which contribute to the averaged behavior of the ensemble.

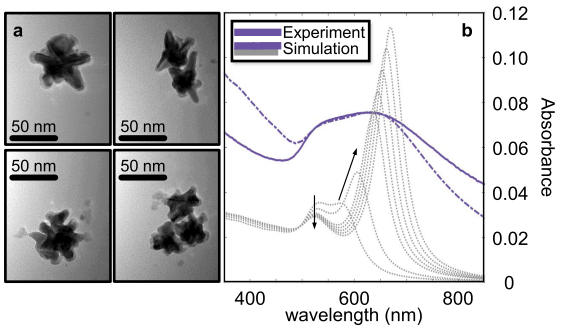

Figure 1. Plasmonic s-NP static optical response. (a) TEM images of the Au s-NPs in an aqueous environment. (b) Experimental (solid) and simulated (dash-dotted) static absorbance of the sample. Gray dotted curves are the simulated absorbance spectra (rescaled in intensity) of virtual s-NP subsets, assuming the absence of inhomogeneous broadening (i.e., disregarding the shape dispersion effects) for s-NPs with tip lengths of 50, 70, 90, 85, 100, 105, 110, and 120% (from the least to the most intense, the trend of the two plasmon modes being also indicated by arrows) of the value considered in the simulations of the whole sample.

To characterize the optical response of the sample under static, unperturbed, conditions, its absorbance was measured as a function of the excitation wavelength λ, that is, the quantity $A(\lambda) = -\log_{10}[T(\lambda)]$, with $T(\lambda)$ being its transmission. The spectrum of $A(\lambda)$, shown in Figure 1b (solid line) over a broad spectral region in the visible, exhibits a clear resonant behavior. A main peak at ∼640 nm is observed, accompanied by a shoulder at higher energies, peaked at ∼540 nm. The two resonant features appear both relatively broad, due to size and shape dispersion of NPs within the sample. Each NP absorbs at slightly shifted peaks depending on its specific morphology, causing the inhomogeneous broadening of the plasmonic resonances in the ensemble.[49] Despite this fact, the measured spectrum is in agreement with previous reports.[37,50] Specifically, theory has rationalized the two resonant modes of highly branched NPs in terms of the hybridization of plasmons associated with the core and the individual tips of the s-NP.[33] In this picture, we interpret the shoulder at 540 nm as a

https://doi.org/10.1021/acs.jpcc.3c07267
J. Phys. Chem. C 2024, 128, 2551−2560

quasistatic-like LSPR arising from the s-NP spherical core and the resonant feature at 640 nm as the low-energy bonding s-NP mode, mainly (although not exclusively[33]) composed of tip plasmons. The core also serves as nanoscale antenna, promoting large electromagnetic field enhancements and an increased extinction of the tip plasmons.

To reproduce numerically the static optical behavior of the whole sample, a reduced model was developed, neglecting the size and shape dispersion of the s-NPs and describing the solution as an ensemble of monodisperse effective s-NPs. As mentioned in the Materials and Methods, this assumption required to introduce an increased Drude damping factor in the Au permittivity[37] to mimic the experimental inhomogeneous spectral broadening. Then, starting from the extinction cross-section of a single isotropic s-NP computed with our FEM-based model, the sample absorbance was simulated and compared with measurements, achieving an accurate estimation of the resonance spectral position and a good quantitative matching (Figure 1b, dash-dotted line). By assuming instead the absence of inhomogeneous broadening (setting the nominal Drude damping for Au), much narrower peaks arise (Figure 1b, gray dotted lines). Under these conditions, the model simulates de facto the response of virtual subsets of s-NPs, featuring varying shapes and sizes within the solution. In line with previous reports,[35] simulations indicate that while the mode promoted by the spherical core is almost independent of the s-NP morphology, the peak regulated by the tips (at longer wavelengths) is extremely sensitive to minor geometrical changes: the spectra in Figure 1b refer to s-NP subsets differing in tip length by a factor between 0.5 and 1.2 compared to the effective s-NP mimicking the whole sample (Figure 1b, purple dash-dotted). More generally, the tip length, aperture angle, and number have a substantial impact on the resonance amplitude and spectral position,[35] representing some versatile degrees of freedom to tune the low-energy LSPR even more effectively compared to more standard geometries with comparable response, such as, e.g., rods.[22,37]

Moreover, our model allows us to provide further insights into the sample optical response, based on the analysis of the effective s-NP behavior. In particular, Figure 2a displays the computed s-NP absorption (σ_{ABS}) and scattering (σ_{SCA}) cross sections which, summed up, give the total extinction. By comparing the resulting spectra (green and black curves, respectively), absorption is shown to dominate the s-NP response (note the magnification factor for σ_{SCA}), contributing to the resonant modes more than scattering, which rather acts as a background. Additionally, with the full-vectorial FEM electromagnetic simulations developed, we could inspect the spatial patterns of the near fields across the s-NP. Specifically, Figure 2b,c reports the space distribution of the electric field enhancement across the individual s-NP at the wavelengths corresponding to the two LSPRs, i.e., λ = 640 nm (Figure 2b) and λ = 540 nm (Figure 2c), confirming the expected NP behavior. At λ = 640 nm (Figure 2b), a strong localization of the field is observed at the spike tips, which behave as electromagnetic hot spots, promoting a significant field enhancement. On the other hand, the field spatial pattern at λ = 540 nm (Figure 2c) is substantially less localized at the spike tips, reminiscent of the typical field distribution across a nanosphere.[42]

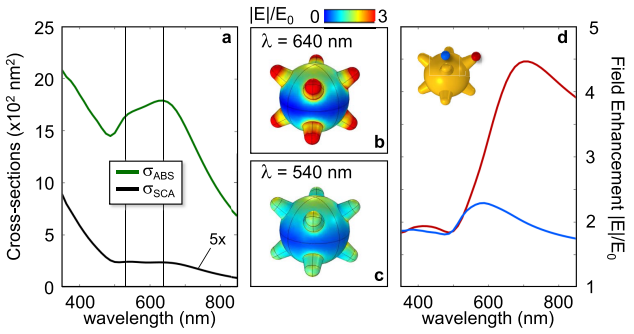

Figure 2. Modeling Au s-NPs. (a) Simulated absorption (green) and scattering (black, magnified for better reading) cross sections of the effective s-NP mimicking the sample. (b,c) Field enhancement distribution across the s-NP surface for the wavelengths λ = 640 nm (b) and λ = 540 nm (c), highlighted as vertical black lines in panel (a). A linearly polarized plane wave along the vertical direction is considered. (d) Spectra of the field enhancement evaluated at two different spatial positions of the s-NP, either at a spike tip (red) or close to the spherical core surface (blue), as sketched in the top left inset.

The notable dependence on the excitation wavelength of the field enhancement can be further visualized by analyzing the spectra of the local electric field (normalized to the incident field E_0) at the NP surface. This quantity is of particular relevance, e.g., for photochemical applications with hot electrons, which benefit from the intense near fields at the NP surface. As an example, Figure 2d reports the spectral trends of the enhancement factor evaluated either at the spike tip (red curve) or at the spherical core pole (blue curve). Consistently, the tip case exhibits a higher amplitude compared to the core one over the entire spectrum, and its peak, dictated by the low-energy spike plasmons, is red-shifted compared to one observed at the core surface.

To characterize the nonlinear behavior of the s-NPs, we employed pump−probe spectroscopy and modeled the Au optical nonlinearities governed by hot carriers (details in the Materials and Methods), examining how the static resonances are modulated upon photoexcitation with ultrashort laser pulses. For a comprehensive investigation of the dynamical nonlinear processes at play, we explored two light−matter interaction regimes by tuning the pump pulse wavelength either off- and on-resonance with the tip LSPR. In the former case, all the s-NPs in the solution have essentially the same response, regardless of their specific morphology. The observed optical behavior is therefore that of the whole ensemble. In the latter, resonant case, the selective excitation of the s-NP subset with a narrow absorption peak at the pump wavelength is expected instead to dominate the observed response.

For the nonresonant case, we set the pump wavelength at 400 nm, i.e., far enough from both of the two resonances (the near fields do not exhibit any resonant pattern, see Figure S1) and explored a range of excitation levels, varying the pump pulse energy to span values of fluence over almost 1 order of magnitude, starting from a relatively weak perturbation regime (yet without exceeding the typical damage threshold of Au nanostructures, see Supporting Information Section S2). Such an approach enabled us to systematically assess the contributions to the optical modulation arising from each of the two LSPRs and to evaluate their relative weight as a function of fluence.

The main results of our experiments are shown in Figure 3a−d, which report the differential transmittance $\Delta T/T$ maps

https://doi.org/10.1021/acs.jpcc.3c07267
J. Phys. Chem. C 2024, 128, 2551−2560

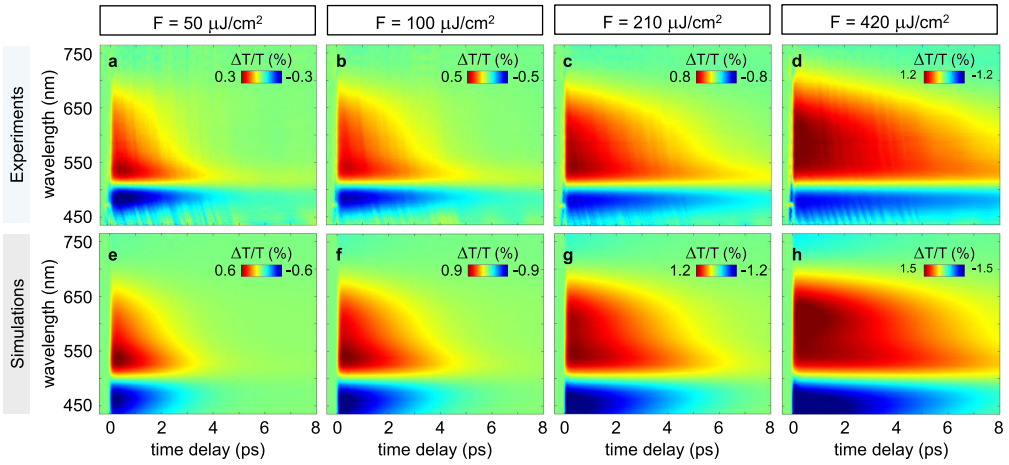

Figure 3. Transient absorption spectroscopy. Experimental (a–d) and simulated (e–h) pump–probe maps of the differential transmittance $\Delta T/T$ of plasmonic s-NPs in an aqueous environment, by varying the excitation level. The pump pulse, centered at λ_p = 400 nm and with temporal duration of ∼100 fs, has fluence (from left to right) F of 50 (a,e), 100 (b,f), 210 (c,g), and 420 μJ/cm^2 (d,h).

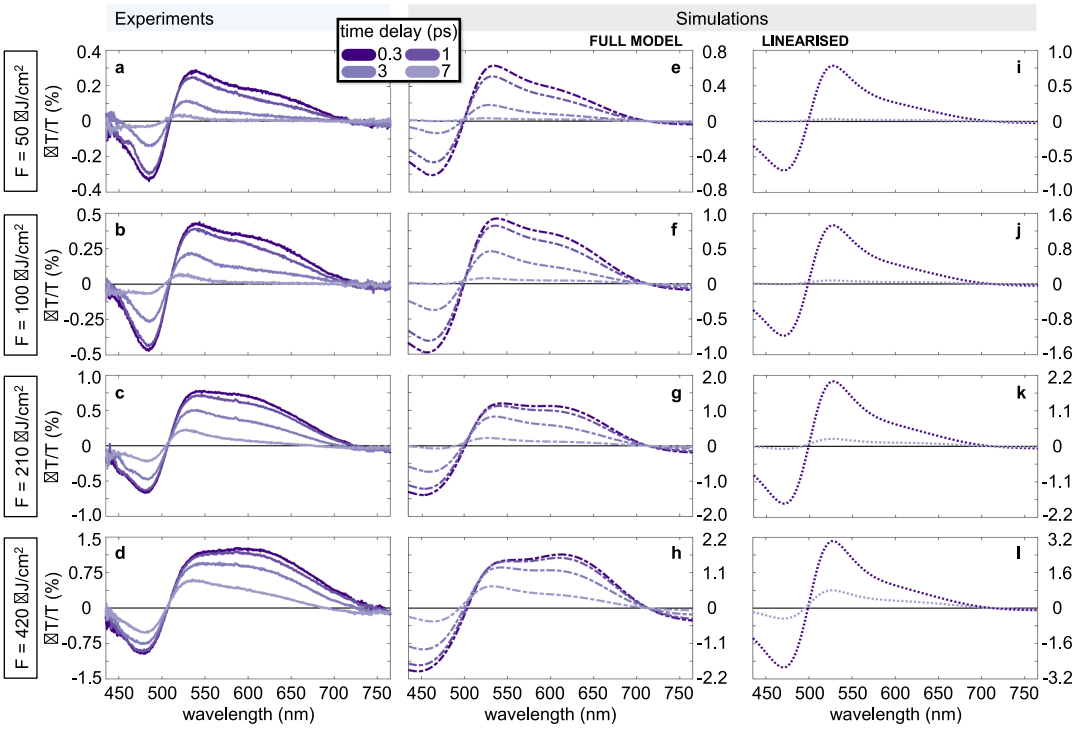

Figure 4. Transient spectra of the broadband differential transmittance signal $\Delta T/T$. Experimental (a–d) and simulated (e–h) $\Delta T/T$ spectra at selected pump–probe time delays of 0.3, 1, 3, and 7 ps (from darker to lighter color shades). (i–l) Same as (e–h) by employing a linearized description of the thermalized electron photoexcitation for time delays of 0.3 and 7 ps.

as a function of the pump–probe time delay and the probe wavelength over a broad spectral range. Four sets of measurements are shown, corresponding to pump fluences F of ∼50, 100, 210, and 420 μJ/cm^2 (in Figure 3a–d, respectively). Experiments are compared with simulations, which are shown in Figure 3e–h for the same values of fluence. Numerical results exhibit good agreement with the measured $\Delta T/T$ apart from a slight mismatch of the signal decay time, possibly due to the misevaluation of the thermal impedance at the s-NP surface (we considered perfect thermal contact, i.e., zero interface thermal resistance), governing the heat transfer from Au to the environment on the ps timescale,[51] which alternative, approximated,[12] or more advanced[52] modeling approaches could more accurately account for. On the other hand, note that our inhomogeneous variant of the 3TM (see the Materials and Methods section) allows us to account for the actual s-NP morphology. Possible impact of the structure geometry on the dynamical evolution of the model energetic variables is thus accurately included, although a weak effect of the intraparticle electronic/thermal diffusion is expected for the specific effective s-NP we considered in the model, as distortion of the ultrafast optical dynamics has been shown to typically require larger nanostructures with controlled orientation.[45]

As observed by comparing the trend of the optical modulation at different fluences (cfr. panels of Figure 3 from

https://doi.org/10.1021/acs.jpcc.3c07267
J. Phys. Chem. C 2024, 128, 2551−2560

left to right), the $\Delta T/T$ pump−probe maps exhibit an overall similar behavior. A broadband positive lobe between 505 and ∼700 nm (this value tending to red shift for increasing pump fluence) is observed, together with two negative bands, at shorter (below 505 nm) and longer (above 700 nm) wavelengths, the latter being much weaker in all cases. This spectral structure precisely matches what was previously reported for comparable systems (in particular, colloidal solutions of Au rods with a low aspect ratio[53]), but it extends over a particularly broad range of wavelengths. Such a broadband modulation, although dominated by the static inhomogeneous broadening, is in fact also influenced by the morphology of the individual NP. For instance, we predicted that nanospheres with the same volume as s-NPs give a narrower modulation band, even for the same extent of broadening under static conditions (see Supporting Information Section S3). Moreover, we note that, for all fluences, simulations tend to predict higher (almost doubled) values of the differential transmittance (compare upper and lower panels in Figure 3), a mismatch ascribed to the overestimation of the sample static absorbance at the pump wavelength.

Although providing qualitatively similar results, both experiments and simulations exhibit substantial variations in the differential transmittance signal when fluence is increased, both in the dynamics and spectra of the $\Delta T/T$. Regarding the temporal evolution of the transient signal, a higher fluence results in a slower decay of the modulation, lasting up to tens of ps for the highest fluence (Figure 3d,h, shown up to 8 ps). This observation is in agreement with previous reports of comparable samples,[54,55] and well explained by our model (see Supporting Information Section S4 for details on the direct impact of increasing the pump fluence on the dynamics of the energetic variables of the 3TM). Within the first few ps, our $\Delta T/T$ is dominated by the relaxation dynamics of thermalized hot carriers (further details in Supporting Information Section S5), fully characterized by their out-of-equilibrium temperature, Θ_E. When the pump pulse fluence increases, the temporal relaxation of Θ_E, governed by eq 2, is known[56] to scale sublinearly and tends to become linear in time, as a result of the dependence on temperature of the electronic heat capacity, C_E (essentially linear, in our excitation regime[57]). A higher heat capacity corresponds indeed to a larger thermal inertia of the hot electrons, which takes therefore more time to exchange energy and, specifically, to equilibrate with the (colder) metal lattice. Besides changes in the signal dynamics, a relevant difference in the $\Delta T/T$ maps is the spectral distortion observed within the first ps when increasing the pump fluence. The high-energy negative lobes and the isosbestic points remain almost unvaried. On the contrary, both in experiments and simulations, the broadband positive lobe does not preserve its spectral structure. To better visualize the changes in the $\Delta T/T$ spectra, Figure 4 reports spectral cuts of the pump−probe maps at selected time delays for the four values of fluence considered. The experimental spectra (Figure 4a−d) show that the broad positive band can be interpreted as the superposition of two lobes, each of which arises from the modulation (shift and broadening, most generally) of one of the two static resonant modes (see also Figure S6). In these terms, the spectral distortion can be understood as a fluence-dependent variation in the relative weights of each of these two spectrally distinct contributions. As the fluence grows, the modulation of the s-NP tip resonance (around 630 nm) experiences a stronger increase, dominating over the modulation of the s-NP core one (close to 530 nm). This peculiar trend is accurately reproduced by our simulations (Figure 4e−h), explaining the experiments in terms of the Au optical nonlinearity governing the transient response, mainly dominated by the so-called Fermi smearing mechanism.[48,58] The photoexcited state of the thermalized electrons can be described by the Fermi−Dirac distribution $f(E,\Theta_E) = [1 + e^{(E-E_F)/k_B\Theta_E}]^{-1}$, with E_F being the Fermi energy and k_B being the Boltzmann constant. When the electronic temperature is higher than room temperature Θ_0 (even up to thousands of K), $f(E,\Theta_E)$ tends indeed to smear in energy, modifying the occupancy probabilities above and below the Fermi level, and, as a result, the interband absorption profile and metal permittivity. The latter inherits a highly nonlinear dependence on Θ_E, thus exhibiting major spectral distortions when Θ_E increases. The main effect is a permittivity reduction (on average) near the Au interband transitions, i.e., close to the s-NP core mode, and an increase at lower energies, where instead the s-NP tips support the plasmon.[54] This mechanism results in the sublinear dependence of $\Delta T/T$ on the pump fluence representing the saturation of the resonance modulation, stronger for the high-energy one as compared to that for the low-energy mode. To ascertain that the observed behavior is due to the nonlinearities introduced by the Fermi smearing, we compared our simulations with the numerical results obtained by linearizing the model for the variation of the hot electron distribution.[58] In formulas, instead of considering the change in the Fermi−Dirac energy distribution of thermalized carriers as given, at each time instant, by the rigorous difference $\Delta f(E,\Theta_E) = f(E,\Theta_E) - f(E,\Theta_0)$, we expressed it as a linear function of $\Delta\Theta_E$, that is $\Delta f(E,\Theta_E) = \left[\frac{\partial f(E,\Theta_E)}{\partial E}\right]_{\Theta_E=\Theta_0^*} \Delta\Theta_E$, with Θ_0^* being an effective room temperature for Θ_E, fitted to mimic the broadening effects in Au interband transitions.[59] As such, the linearized model treats Δf as if it had an unvaried distribution in energy, modulated in time by the dynamical evolution of the electronic temperature throughout the photoexcitation. The spectra of the differential transmittance obtained by following such a linearized approach are reported in Figure 4i−l and, as a result of considering a time-independent energy spectrum of the electron distribution, do not show any distortion over time. The clear mismatch with the experimental traces evidence that a fully nonperturbative model of the optical nonlinearities introduced by the Fermi smearing is essential to capture the system response on ultrafast timescales.

To complement our analysis, we repeated our pump−probe experiments for an excitation wavelength of 660 nm, i.e., close to the peak ascribed to the tip mode in the ensemble static absorbance. Under these conditions, the pump pulse is expected to excite the whole sample, yet experiencing a stronger interaction with the subset of s-NPs which exhibit the tip-mediated resonance precisely at λ_p. This translates into a preferential excitation of such a subset and a corresponding favored pump photon energy absorption by those NPs.[53] Note that an equivalent behavior is not expected for a pump excitation resonant with the core-mediated mode (i.e., ∼540 nm, Figure 2c), which is much less sensitive to slight morphological changes of the NPs within the ensemble, hence (similarly to the 400 nm-pump) not suitable for driving selective processes. Figure 5a visually depicts this interaction mechanism, where the narrow response of a virtual subset of

https://doi.org/10.1021/acs.jpcc.3c07267
J. Phys. Chem. C 2024, 128, 2551−2560

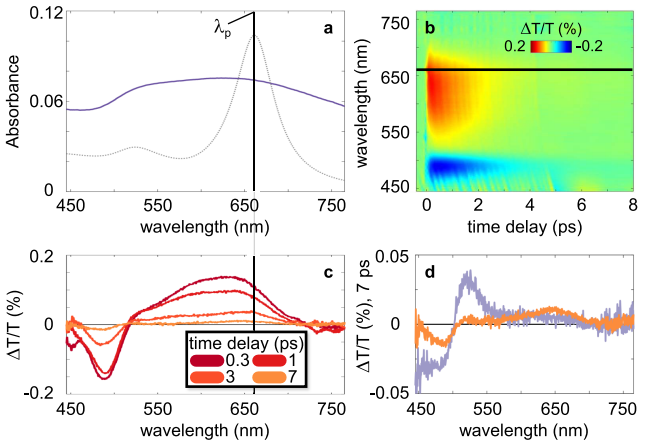

Figure 5. Resonant, selective pump−probe experiments. (a) Measured static absorbance of the sample (purple) and of the simulated virtual subset (scaled in intensity) of s-NPs selectively excited by the pump (gray dotted). The black line highlights the spectral position of the pump wavelength λ_p = 660 nm. (b) Experimental pump−probe map of the differential transmittance $\Delta T/T$. Pump fluence was set ∼25 $\mu J/cm^2$ to have a transient signal of the same magnitude as the off-resonant experiments with the lowest fluence. (c) Spectral cuts of the measured $\Delta T/T$ at selected pump−probe time delays of 0.3, 1, 3, and 7 ps (from darker to lighter color shades). (d) Comparison of the $\Delta T/T$ spectra at a long pump−probe delay (7 ps) for either the on-resonance (purple, pump fluence 50 $\mu J/cm^2$) or off-resonance (orange) pump excitation case.

NPs selectively interacting with the pump is taken out from the measured, much broader absorbance of the polydisperse sample. In the transient regime, the measured pump−probe signal (Figure 5b) shows major changes in its spectral shape when tuning the pump wavelength on- rather than off-resonance with the tip mode. The overall dynamics (relaxation within a few ps) and spectral structure (a main positive lobe between 500 and 700 nm, accompanied by two lateral negative lobes) is preserved.[55] However, the positive lobe is more intense around 660 nm (especially at longer delays), and the modulation of the tip LSPR gets both larger in amplitude and spectrally broader compared to the 400 nm-pump case, causing a marked spectral distortion of the whole lobe. Such a trend is further evidenced by comparing the shapes of the signal in the $\Delta T/T$ cuts in Figure 5d (experiments with signals of similar magnitude). For a full spectral side-by-side comparison, see Supporting Information Section S6.

This effect is interpreted as the fingerprint of the s-NP subset resonant with λ_p, the contribution of which now dominates the transient optical signal. Indeed, the selective photon energy delivery to these NPs produces an inhomogeneously excited ensemble, featuring a transient response where the relative weights of each subset do not follow their population (as in the linear regime), but depend on the pump-induced excitation level. Such pump-selective process is not induced with a 400 nm pump wavelength, when, on the contrary, all s-NPs absorb approximately the same amount of pump photon energy. Their absorbance does not depend crucially on their morphology in this spectral region, making the 400 nm excitation mostly homogeneous within the solution. As such, the resulting transient behavior is the superposition of identical responses from all s-NP subsets, weighted as in the stationary spectrum.[53] Note that the dependence on the preferential pump excitation of the transient spectra, also discussed for similar colloidal solutions of nanorods,[53,55] is not limited to our sample. More generally, any polydisperse sample with a multimodal response and an optical resonance featuring high shape sensitivity could be suitable, indicating ample versatility of the colloidal platform proposed here for all-optical spectral shaping. Moreover, inspecting the absorbance of the considered virtual subset (Figure 5a, gray curve), respectively, at 400 and 660 nm suggests that absorption is substantially larger at the latter wavelength (almost by three times) than the former. This corresponds, in the transient regime, to a higher internal excitation level (in particular, a higher electronic temperature) reached by the s-NPs pumped at 660 nm compared to the 400 nm case, hence to a more pronounced Fermi smearing.[55,58] In these terms, we interpret the distortion in the $\Delta T/T$ of Figure 5d as related also to the increased broadening due to the nonlinear Fermi smearing, being stronger on- than off-resonance.

Simulating the response of the sample upon resonant pumping would require to account for a macroscale inhomogeneous distribution of s-NP morphologies within the sample, beyond the approximated approach of employing a monodisperse effective NP ensemble. Each s-NP subset narrow response should be considered and averaged in the transient regime to reproduce the sample behavior. While a rigorous description of such ensemble effects falls out of the scope of our modeling here discussed, future works employing, e.g., Monte Carlo approaches or targeted large-scale methods[60] to account for disorder within the NP solution could be envisaged. This could lead to gain insight into effects beyond the pump-selection process we observed here, for instance related to transient photoinduced anisotropy or orientation-dependent interactions in complex NP geometries. In parallel, single-particle spectroscopy investigating the ultrafast dynamics of plasmonic nanostructures[25,46,61] could shed light on the nonlinear behavior of individual nano-objects with complex shapes.

CONCLUSIONS

In summary, in this study, we have examined the early stages of the transient nonlinear optical response of plasmonic nanostars. Our sample, consisting of a polydisperse ensemble of Au s-NPs, exhibited a bimodal static absorbance affected by the inhomogeneous broadening of the single NP plasmon resonances. Femtosecond pump−probe spectroscopy and a quantitative time-resolved model of the hot carrier dynamics were combined to study the ultrafast energy relaxation of the s-NPs electronic population and inherent optical nonlinearities. We considered two photoexcitation conditions, either off- or on-resonance with the plasmonic mode regulated by hot spots, demonstrating a pump-selective spectral shaping of the transient optical signal.

Pumping off-resonance (λ_p = 400 nm) entails a homogeneous excitation of the whole ensemble, thus providing insight into the collective behavior of the sample. Under these conditions, the transient modulations of the two LSPRs were shown to have different relative weights. As a function of the pump pulse fluence, we observed a saturation effect, fingerprint of the nonlinear Fermi smearing in the metal, which is more pronounced for the core resonance at shorter wavelengths. On the other side, tuning the pump to match the tip-resonance (λ_p = 660 nm) promotes a selective excitation of the sample. Energy is preferentially delivered to specific s-NP subsets,

https://doi.org/10.1021/acs.jpcc.3c07267
J. Phys. Chem. C 2024, 128, 2551−2560

depending on their morphology and hot spots. Major distortions in the spectra of the differential transmittance were observed, due to the modified relative contributions of each subset to the transient response.

Our results resolve the ultrafast response of hot carriers in colloidal nanostars, contributing to the understanding of the nonlinear mechanisms mediated by plasmonic tips. This could advance the development of nanosystems for an optimal exploitation of electromagnetic hot spots, e.g., in hot carrier-based photocatalytic platforms,[37,62] biological and chemical sensors,[63] or surface-enhanced Raman spectroscopy,[14] outperforming more conventional shapes. Moreover, the demonstration of the reshaping of transient spectra with the excitation wavelength might lead to ultrafast all-optical plasmonic modulators enabling to selectively manipulate light over a broad bandwidth. High-speed optical switches or ultrafast photodetectors could benefit from nanophotonic active platforms reconfigured by all-optical means, with potential interest ranging from free-space optics to optoelectronics. Since the process is of general validity and ultimately regulated by the photoexcitation of hot carriers, all-dielectric nanostructures could be also envisaged, featuring reduced losses compared to that observed in plasmonic materials. Finally, our analysis could be of relevance also beyond purely electromagnetic phenomena. For instance, by employing suitable materials with high electron−phonon coupling (such as TiN[64] or HfN[65]), an ultrafast thermal imprinting of hot spots can be achieved. This could open routes toward the engineering of subwavelength transient heat management,[66] with potential impact in, e.g., biomedical[67] or solar thermal applications,[68] where s-NPs could serve as efficient nanoheaters with broad optical tunability.

■ ASSOCIATED CONTENT

Supporting Information

The Supporting Information is available free of charge at https://pubs.acs.org/doi/10.1021/acs.jpcc.3c07267.

Off-resonant pump absorption pattern; nanoparticle photoinduced reshaping; ultrafast simulations on plasmonic nanospheres; modeling the nonequilibrium dynamics of plasmonic nanostructures; disentangling the ultrafast nonlinear response of plasmonic nanostars; nonlinear saturation effect; and tuning the pump wavelength: a side-by-side comparison (PDF)

■ AUTHOR INFORMATION

Corresponding Author

Margherita Maiuri − *Dipartimento di Fisica, Politecnico di Milano, I-20133 Milano, Italy; Istituto di Fotonica e Nanotecnologie − Consiglio Nazionale delle Ricerche, I-20133 Milano, Italy;* orcid.org/0000-0001-9351-8551; Email: margherita.maiuri@polimi.it

Authors

Andrea Schirato − *Dipartimento di Fisica, Politecnico di Milano, I-20133 Milano, Italy; Istituto Italiano di Tecnologia, 16163 Genoa, Italy;* orcid.org/0000-0001-8024-9778

Luca Moretti − *Dipartimento di Fisica, Politecnico di Milano, I-20133 Milano, Italy; Istituto di Fotonica e Nanotecnologie − Consiglio Nazionale delle Ricerche, I-20133 Milano, Italy;* orcid.org/0000-0001-8092-0752

Elisa Lacroce − *Dipartimento di Chimica, Materiali, Ingegneria Chimica Giulio Natta, Politecnico di Milano, 20131 Milan, Italy*

Laura Polito − *Consiglio Nazionale delle Ricerche, CNR-SCITEC, 20138 Milan, Italy;* orcid.org/0000-0002-7756-2365

Filippo Rossi − *Dipartimento di Chimica, Materiali, Ingegneria Chimica Giulio Natta, Politecnico di Milano, 20131 Milan, Italy;* orcid.org/0000-0003-2665-120X

Giuseppe Della Valle − *Dipartimento di Fisica, Politecnico di Milano, I-20133 Milano, Italy; Istituto di Fotonica e Nanotecnologie − Consiglio Nazionale delle Ricerche, I-20133 Milano, Italy;* orcid.org/0000-0003-0117-2683

Complete contact information is available at: https://pubs.acs.org/10.1021/acs.jpcc.3c07267

Author Contributions

[I]A. Schirato and L. Moretti contributed equally.

Funding

A.S., G.D.V., and M.M. acknowledge financial support by the European Union's NextGenerationEU Programme with the I-PHOQS Infrastructure [IR0000016, ID D2B8D520, CUP B53C22001750006] "Integrated infrastructure initiative in Photonic and Quantum Sciences". This publication was part of the METAFAST project that received funding from the European Union Horizon 2020 Research and Innovation program under grant agreement no. 899673. This work reflects only author view, and the European Commission was not responsible for any use that may be made of the information it contains. G.D.V. acknowledges the support from the HOTMETA project under the PRIN 2022 MUR program funded by the European Union − Next Generation EU − "PNRR − M4C2, investimento 1.1 − "Fondo PRIN 2022" - HOT-carrier METasurfaces for Advanced photonics (HOT-META), contract no. 2022LENW33 − CUP: D53D2300229 0006".

Notes

The authors declare no competing financial interest.

■ REFERENCES

(1) Maier, S. A.; Brongersma, M. L.; Kik, P. G.; Meltzer, S.; Requicha, A. A. G.; Atwater, H. A. Plasmonics—A Route to Nanoscale Optical Devices. *Adv. Mater.* **2001**, *13* (19), 1501−1505.

(2) Schuller, J. A.; Barnard, E. S.; Cai, W.; Jun, Y. C.; White, J. S.; Brongersma, M. L. Plasmonics for extreme light concentration and manipulation. *Nat. Mater.* **2010**, *9* (3), 193−204.

(3) Liz-Marzán, L. M.; Murphy, C. J.; Wang, J. Nanoplasmonics. *Chem. Soc. Rev.* **2014**, *43* (11), 3820−3822.

(4) Maier, S. A. *Plasmonics: Fundamentals and Applications*. 1st ed. 2007. ed.; Springer US: New York, NY, 2007.

(5) Link, S.; El-Sayed, M. A. Shape and size dependence of radiative, non-radiative and photothermal properties of gold nanocrystals. *Int. Rev. Phys. Chem.* **2000**, *19* (3), 409−453.

(6) Jain, P. K.; Huang, X.; El-Sayed, I. H.; El-Sayed, M. A. Noble Metals on the Nanoscale: Optical and Photothermal Properties and Some Applications in Imaging, Sensing, Biology, and Medicine. *Acc. Chem. Res.* **2008**, *41* (12), 1578−1586.

(7) Chaâbani, W.; Proust, J.; Ouellet, S.; Movsesyan, A.; Béal, J.; Bachelot, R.; Xu, T.; Baudrion, A.-L.; Adam, P.-M.; Boudreau, D.; Chehaidar, A.; Plain, J. Si@Au Core-Shell Nanostructures: Toward a New Platform for Controlling Optical Properties at the Nanoscale. *J. Phys. Chem. C* **2021**, *125* (37), 20606−20616.

(8) Wang, H.-J.; Lin, J.-S.; Zhang, H.; Zhang, Y.-J.; Li, J.-F. Plasmonic Core-Shell Materials: Synthesis, Spectroscopic Character-

ization, and Photocatalytic Applications. *Acc. Mater. Res.* **2022**, *3* (2), 187−198.
(9) Halas, N. J.; Lal, S.; Chang, W.-S.; Link, S.; Nordlander, P. Plasmons in Strongly Coupled Metallic Nanostructures. *Chem. Rev.* **2011**, *111* (6), 3913−3961.
(10) Kim, D. Y.; Yu, T.; Cho, E. C.; Ma, Y.; Park, O. O.; Xia, Y. Synthesis of Gold Nano-hexapods with Controllable Arm Lengths and Their Tunable Optical Properties. *Angew. Chem., Int. Ed.* **2011**, *50* (28), 6328−6331.
(11) Movsesyan, A.; Santiago, E. Y.; Burger, S.; Correa-Duarte, M. A.; Besteiro, L. V.; Wang, Z.; Govorov, A. O. Plasmonic Nanocrystals with Complex Shapes for Photocatalysis and Growth: Contrasting Anisotropic Hot-Electron Generation with the Photothermal Effect. *Adv. Opt. Mater.* **2022**, *10* (10), 2102663.
(12) Schirato, A.; Moretti, L.; Yang, Z.; Mazzanti, A.; Cerullo, G.; Pileni, M.-P.; Maiuri, M.; Della Valle, G. Chemically-Controlled Ultrafast Photothermal Response in Plasmonic Nanostructured Assemblies. *J. Phys. Chem. C* **2022**, *126* (14), 6308−6317.
(13) Liu, Q.; Ge, D.; Wackenhut, F.; Coplan, C. D.; Cherqui, C.; Brecht, M.; Lin, X.-M.; Schatz, G. C.; Schaller, R. D.; Adam, P.-M.; Bachelot, R.; Meixner, A. J. Revealing the Three-Dimensional Orientation and Interplay between Plasmons and Interband Transitions for Single Gold Bipyramids by Photoluminescence Excitation Pattern Imaging. *J. Phys. Chem. C* **2021**, *125* (48), 26978−26985.
(14) Tanwar, S.; Haldar, K. K.; Sen, T. DNA Origami Directed Au Nanostar Dimers for Single-Molecule Surface-Enhanced Raman Scattering. *J. Am. Chem. Soc.* **2017**, *139* (48), 17639−17648.
(15) Tian, F.; Conde, J.; Bao, C.; Chen, Y.; Curtin, J.; Cui, D. Gold nanostars for efficient in vitro and in vivo real-time SERS detection and drug delivery via plasmonic-tunable Raman/FTIR imaging. *Biomaterials* **2016**, *106*, 87−97.
(16) Kim, W.; Kim, N.; Park, J. W.; Kim, Z. H. Nanostar probes for tip-enhanced spectroscopy. *Nanoscale* **2016**, *8* (2), 987−994.
(17) Garcia-Leis, A.; Garcia-Ramos, J. V.; Sanchez-Cortes, S. Silver Nanostars with High SERS Performance. *J. Phys. Chem. C* **2013**, *117* (15), 7791−7795.
(18) Liu, Y.; Yuan, H.; Fales, A.; Register, J.; Vo-Dinh, T. Multifunctional gold nanostars for molecular imaging and cancer therapy. *Front. Chem.* **2015**, *3*..
(19) Espinosa, A.; Silva, A. K. A.; Sánchez-Iglesias, A.; Grzelczak, M.; Péchoux, C.; Desboeufs, K.; Liz-Marzán, L. M.; Wilhelm, C. Cancer Cell Internalization of Gold Nanostars Impacts Their Photothermal Efficiency In Vitro and In Vivo: Toward a Plasmonic Thermal Fingerprint in Tumoral Environment. *Adv. Healthcare Mater.* **2016**, *5* (9), 1040−1048.
(20) Chatterjee, H.; Rahman, D. S.; Sengupta, M.; Ghosh, S. K. Gold Nanostars in Plasmonic Photothermal Therapy: The Role of Tip Heads in the Thermoplasmonic Landscape. *J. Phys. Chem. C* **2018**, *122* (24), 13082−13094.
(21) Atta, S.; Pennington, A. M.; Celik, F. E.; Fabris, L. TiO2 on Gold Nanostars Enhances Photocatalytic Water Reduction in the Near-Infrared Regime. *Chem* **2018**, *4* (9), 2140−2153.
(22) Cushing, S. K.; Chen, C.-J.; Dong, C. L.; Kong, X.-T.; Govorov, A. O.; Liu, R.-S.; Wu, N. Tunable Nonthermal Distribution of Hot Electrons in a Semiconductor Injected from a Plasmonic Gold Nanostructure. *ACS Nano* **2018**, *12* (7), 7117−7126.
(23) Sousa-Castillo, A.; Comesaña-Hermo, M.; Rodríguez-González, B.; Pérez-Lorenzo, M.; Wang, Z.; Kong, X.-T.; Govorov, A. O.; Correa-Duarte, M. A. Boosting Hot Electron-Driven Photocatalysis through Anisotropic Plasmonic Nanoparticles with Hot Spots in Au-TiO2 Nanoarchitectures. *J. Phys. Chem. C* **2016**, *120* (21), 11690−11699.
(24) Nan, L.; Giráldez-Martínez, J.; Stefancu, A.; Zhu, L.; Liu, M.; Govorov, A. O.; Besteiro, L. V.; Cortés, E. Investigating Plasmonic Catalysis Kinetics on Hot-Spot Engineered Nanoantennae. *Nano Lett.* **2023**, *23* (7), 2883−2889.
(25) Crut, A.; Maioli, P.; Del Fatti, N.; Vallée, F. Optical absorption and scattering spectroscopies of single nano-objects. *Chem. Soc. Rev.* **2014**, *43* (11), 3921−3956.
(26) Catone, D.; Di Mario, L.; Martelli, F.; O'Keeffe, P.; Paladini, A.; Stefano Pelli Cresi, J.; Sivan, A. K.; Tian, L.; Toschi, F.; Turchini, S. Ultrafast optical spectroscopy of semiconducting and plasmonic nanostructures and their hybrids. *Nanotechnology* **2020**, *32* (2), 025703.
(27) Maiuri, M.; Garavelli, M.; Cerullo, G. Ultrafast Spectroscopy: State of the Art and Open Challenges. *J. Am. Chem. Soc.* **2020**, *142* (1), 3−15.
(28) Link, S.; El-Sayed, M. A. Optical Properties and Ultrafast Dynamics of Metallic Nanocrystals. *Annu. Rev. Phys. Chem.* **2003**, *54* (1), 331−366.
(29) Conforti, M.; Della Valle, G. Derivation of third-order nonlinear susceptibility of thin metal films as a delayed optical response. *Phys. Rev. B* **2012**, *85* (24), 245423.
(30) Manjavacas, A.; Liu, J. G.; Kulkarni, V.; Nordlander, P. Plasmon-Induced Hot Carriers in Metallic Nanoparticles. *ACS Nano* **2014**, *8* (8), 7630−7638.
(31) Schirato, A.; Maiuri, M.; Cerullo, G.; Della Valle, G. Ultrafast hot electron dynamics in plasmonic nanostructures: experiments, modelling, design. *Nanophotonics* **2023**, *12* (1), 1−28.
(32) Brongersma, M. L.; Halas, N. J.; Nordlander, P. Plasmon-induced hot carrier science and technology. *Nat. Nanotechnol.* **2015**, *10* (1), 25−34.
(33) Hao, F.; Nehl, C. L.; Hafner, J. H.; Nordlander, P. Plasmon Resonances of a Gold Nanostar. *Nano Lett.* **2007**, *7* (3), 729−732.
(34) de Puig, H.; Tam, J. O.; Yen, C.-W.; Gehrke, L.; Hamad-Schifferli, K. Extinction Coefficient of Gold Nanostars. *J. Phys. Chem. C* **2015**, *119* (30), 17408−17415.
(35) Barbosa, S.; Agrawal, A.; Rodríguez-Lorenzo, L.; Pastoriza-Santos, I.; Alvarez-Puebla, R. A.; Kornowski, A.; Weller, H.; Liz-Marzán, L. M. Tuning Size and Sensing Properties in Colloidal Gold Nanostars. *Langmuir* **2010**, *26* (18), 14943−14950.
(36) Wheeler, D. A.; Green, T. D.; Wang, H.; Fernández-López, C.; Liz-Marzán, L.; Zou, S.; Knappenberger, K. L.; Zhang, J. Z. Optical properties and coherent vibrational oscillations of gold nanostars. *Chem. Phys. Lett.* **2012**, *543*, 127−132.
(37) Kong, X.-T.; Wang, Z.; Govorov, A. O. Plasmonic Nanostars with Hot Spots for Efficient Generation of Hot Electrons under Solar Illumination. *Adv. Opt. Mater.* **2017**, *5*(15)..
(38) Santiago, E. Y.; Besteiro, L. V.; Kong, X.-T.; Correa-Duarte, M. A.; Wang, Z.; Govorov, A. O. Efficiency of Hot-Electron Generation in Plasmonic Nanocrystals with Complex Shapes: Surface-Induced Scattering, Hot Spots, and Interband Transitions. *ACS Photonics* **2020**, *7* (10), 2807−2824.
(39) Boyd, R. W.; Shi, Z.; De Leon, I. The third-order nonlinear optical susceptibility of gold. *Opt. Commun.* **2014**, *326*, 74−79.
(40) Silvestri, A.; Lay, L.; Psaro, R.; Polito, L.; Evangelisti, C. Fluidic Manufacture of Star-Shaped Gold Nanoparticles. *Chem.−Eur. J.* **2017**, *23* (41), 9732−9735.
(41) Marelli, M.; Bossola, F.; Spinetti, G.; Sangalli, E.; Santo, V. D.; Psaro, R.; Polito, L. Microfluidic Synthesis of Hybrid TiO2-Anisotropic Gold Nanoparticles with Visible and Near-Infrared Activity. *ACS Appl. Mater. Interfaces* **2020**, *12* (34), 38522−38529.
(42) Bohren, C. F.; Huffman, D. R. *Absorption and scattering of light by small particles/Craig F. Bohren, Donald R. Huffman*; Wiley: Weinheim, Germany, 2004.
(43) Johnson, P. B.; Christy, R. W. Optical Constants of the Noble Metals. *Phys. Rev. B* **1972**, *6* (12), 4370−4379.
(44) Sun, C. K.; Vallée, F.; Acioli, L. H.; Ippen, E. P.; Fujimoto, J. G. Femtosecond-tunable measurement of electron thermalization in gold. *Phys. Rev. B* **1994**, *50* (20), 15337−15348.
(45) Schirato, A.; Maiuri, M.; Toma, A.; Fugattini, S.; Proietti Zaccaria, R.; Laporta, P.; Nordlander, P.; Cerullo, G.; Alabastri, A.; Della Valle, G. Transient optical symmetry breaking for ultrafast broadband dichroism in plasmonic metasurfaces. *Nat. Photonics* **2020**, *14* (12), 723−727.

https://doi.org/10.1021/acs.jpcc.3c07267
J. Phys. Chem. C 2024, 128, 2551−2560

(46) Zavelani-Rossi, M.; Polli, D.; Kochtcheev, S.; Baudrion, A.-L.; Béal, J.; Kumar, V.; Molotokaite, E.; Marangoni, M.; Longhi, S.; Cerullo, G.; Adam, P.-M.; Della Valle, G. Transient Optical Response of a Single Gold Nanoantenna: The Role of Plasmon Detuning. *ACS Photonics* **2015**, *2* (4), 521−529.
(47) Rashidi-Huyeh, M.; Palpant, B. Thermal response of nanocomposite materials under pulsed laser excitation. *J. Appl. Phys.* **2004**, *96* (8), 4475−4482.
(48) Rosei, R. Temperature modulation of the optical transitions involving the Fermi surface in Ag: Theory. *Phys. Rev. B* **1974**, *10* (2), 474−483.
(49) Husnik, M.; Linden, S.; Diehl, R.; Niegemann, J.; Busch, K.; Wegener, M. Quantitative Experimental Determination of Scattering and Absorption Cross-Section Spectra of Individual Optical Metallic Nanoantennas. *Phys. Rev. Lett.* **2012**, *109* (23), 233902.
(50) Nehl, C. L.; Liao, H.; Hafner, J. H. Optical Properties of Star-Shaped Gold Nanoparticles. *Nano Lett.* **2006**, *6* (4), 683−688.
(51) Baffou, G.; Rigneault, H. Femtosecond-pulsed optical heating of gold nanoparticles. *Phys. Rev. B* **2011**, *84* (3), 035415.
(52) Chen, G. Ballistic-Diffusive Heat-Conduction Equations. *Phys. Rev. Lett.* **2001**, *86* (11), 2297−2300.
(53) Wang, X.; Guillet, Y.; Selvakannan, P. R.; Remita, H.; Palpant, B. Broadband Spectral Signature of the Ultrafast Transient Optical Response of Gold Nanorods. *J. Phys. Chem. C* **2015**, *119* (13), 7416−7427.
(54) Silva, M. G.; Teles-Ferreira, D. C.; Siman, L.; Chaves, C. R.; Ladeira, L. O.; Longhi, S.; Cerullo, G.; Manzoni, C.; de Paula, A. M.; Della Valle, G. Universal saturation behavior in the transient optical response of plasmonic structures. *Phys. Rev. B* **2018**, *98* (11), 115407.
(55) Chiang, W.-Y.; Bruncz, A.; Ostovar, B.; Searles, E. K.; Brasel, S.; Hartland, G.; Link, S. Electron-Phonon Relaxation Dynamics of Hot Electrons in Gold Nanoparticles Are Independent of Excitation Pathway. *J. Phys. Chem. C* **2023**, *127*, 21176−21185.
(56) Voisin, C.; Del Fatti, N.; Christofilos, D.; Vallée, F. Ultrafast Electron Dynamics and Optical Nonlinearities in Metal Nanoparticles. *J. Phys. Chem. B* **2001**, *105* (12), 2264−2280.
(57) Lin, Z.; Zhigilei, L. V.; Celli, V. Electron-phonon coupling and electron heat capacity of metals under conditions of strong electron-phonon nonequilibrium. *Phys. Rev. B* **2008**, *77* (7), 075133.
(58) Schirato, A.; Crotti, G.; Gonçalves Silva, M.; Teles-Ferreira, D. C.; Manzoni, C.; Proietti Zaccaria, R.; Laporta, P.; de Paula, A. M.; Cerullo, G.; Della Valle, G. Ultrafast Plasmonics Beyond the Perturbative Regime: Breaking the Electronic-Optical Dynamics Correspondence. *Nano Lett.* **2022**, *22* (7), 2748−2754.
(59) Winsemius, P.; Guerrisi, M.; Rosei, R. Splitting of the interband absorption edge in Au: Temperature dependence. *Phys. Rev. B* **1975**, *12* (10), 4570−4572.
(60) Solís, D. M.; Taboada, J. M.; Obelleiro, F.; Liz-Marzán, L. M.; García de Abajo, F. J. Toward Ultimate Nanoplasmonics Modeling. *ACS Nano* **2014**, *8* (8), 7559−7570.
(61) Baida, H.; Mongin, D.; Christofilos, D.; Bachelier, G.; Crut, A.; Maioli, P.; Del Fatti, N.; Vallée, F. Ultrafast Nonlinear Optical Response of a Single Gold Nanorod near Its Surface Plasmon Resonance. *Phys. Rev. Lett.* **2011**, *107* (5), 057402.
(62) Gargiulo, J.; Berté, R.; Li, Y.; Maier, S. A.; Cortés, E. From Optical to Chemical Hot Spots in Plasmonics. *Acc. Chem. Res.* **2019**, *52* (9), 2525−2535.
(63) Jans, H.; Huo, Q. Gold nanoparticle-enabled biological and chemical detection and analysis. *Chem. Soc. Rev.* **2012**, *41* (7), 2849−2866.
(64) Rotta Loria, S.; Bricchi, B. R.; Schirato, A.; Mascaretti, L.; Mancarella, C.; Naldoni, A.; Li Bassi, A.; Della Valle, G.; Zavelani-Rossi, M. Unfolding the Origin of the Ultrafast Optical Response of Titanium Nitride. *Adv. Opt. Mater.* **2023**, *11* (15), 2300333.
(65) Askes, S. H. C.; Garnett, E. C. Ultrafast Thermal Imprinting of Plasmonic Hotspots. *Adv. Mater.* **2021**, *33* (49), 2105192.
(66) Dongare, P. D.; Zhao, Y.; Renard, D.; Yang, J.; Neumann, O.; Metz, J.; Yuan, L.; Alabastri, A.; Nordlander, P.; Halas, N. J. A 3D Plasmonic Antenna-Reactor for Nanoscale Thermal Hotspots and Gradients. *ACS Nano* **2021**, *15* (5), 8761−8769.
(67) Moretti, L.; Mazzanti, A.; Rossetti, A.; Schirato, A.; Polito, L.; Pizzetti, F.; Sacchetti, A.; Cerullo, G.; Della Valle, G.; Rossi, F.; Maiuri, M. Plasmonic control of drug release efficiency in agarose gel loaded with gold nanoparticle assemblies. *Nanophotonics* **2020**, *10* (1), 247−257.
(68) Rodríguez-Oliveros, R.; Sánchez-Gil, J. A. Gold nanostars as thermoplasmonic nanoparticles for optical heating. *Opt. Express* **2012**, *20* (1), 621−626.

https://doi.org/10.1021/acs.jpcc.3c07267
J. Phys. Chem. C 2024, 128, 2551−2560